Available online at www.sciencedirect.com

ScienceDirect

IFAC Papers Online CONFERENCE PAPER ARCHIVE

IFAC PapersOnLine 59-18 (2025) 43–48

An MRI Compatible Robotics System for Abdominal Intervention ⋆

Hsueh-Yu Chen * **Hsiao-Wen Chung** ** **Chih-Horng Wu** *** **Yu-Hsiu Lee** *

* *Department of Mechanical Engineering, National Taiwan University, Taipei, Taiwan (e-mail: r12522801@ntu.edu.tw, yuhsiulee@ntu.edu.tw)*
** *Department of Electrical Engineering, National Taiwan University, Taipei, Taiwan (e-mail: chunghw@ntu.edu.tw)*
*** *Center of Minimal-Invasive Interventional Radiology, Department of Medical Imaging, National Taiwan University Hospital, Taipei, Taiwan (e-mail: chw1020@ntuh.gov.tw)*

Abstract: Minimally invasive abdominal interventions often require precise needle placement, a challenge magnified by the confined space and magnetic constraints of magnetic resonance imaging (MRI) environments. This study presents an MRI-compatible robotic system featuring a decoupled parallelogram-based Remote Center of Motion (RCM) mechanism for accurate needle angulation and compact design. A pneumatically actuated needle insertion module employing inchworm motion addresses stroke limitations, while a compliant gripper ensures secure and flexible needle manipulation. These innovations enhance procedural accuracy and efficiency, with preliminary results demonstrating the robot's potential for MRI-guided abdominal interventions.

Keywords: MR-conditional robot, minimally invasive surgery, abdominal intervention, mechanism design

1. INTRODUCTION

Abdominal organ cancers, particularly hepatocellular carcinoma (HCC), are the third leading cause of cancer-related deaths worldwide, and their incidence is steadily increasing due to the prevalence of hepatitis C virus infection [Pacella et al. (2011)]. However, up to 90% of patients cannot undergo surgery due to the location and size of the tumor, or physical limitations [Dick et al. (2002)]. Minimally invasive surgery (MIS) employs needle-based techniques, such as biopsies and ablations, which are effective methods for diagnosing or treating abdominal tumors. The precision of needle placement during these procedures is crucial, as incorrect location (less than 1 cm) can lead to a 70% chance of tumor recurrence within 5 years or cause irreversible damage to surrounding organs [Di Costanzo et al. (2014)]. Therefore, leveraging imaging and sensing technologies to enhance needle positioning is key to improving the safety and effectiveness of these treatments. These interventions are guided by medical imaging, with magnetic resonance imaging (MRI) standing out due to its superior soft tissue contrast, higher resolution than ultrasound (US), and the absence of radiation limitations compared to computed tomography (CT), making it ideal for safe and precise localization [Kim et al. (2012)]. However, MRI presents unique challenges during surgery due to the confined space of the scanning chamber and strong magnetic fields. Manual operations become significantly constrained, making the use of robot-assisted surgery increasingly important.

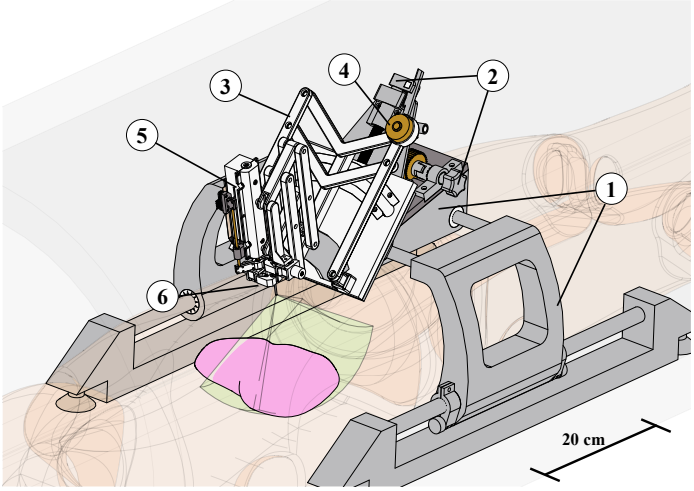

Fig. 1. Schematic diagram of preoperative positioning in the MRI chamber. ① an adjustable bed; ② a handwheel for setting the robot; ③ decoupled parallelogram mechanisms; ④ MRI-compatible ultrasound motor; ⑤ a pneumatic cylinder-actuated needle insertion device; and ⑥ a gripper for holding the needle.

In 2000, Chinzei et al. developed a biopsy robot based on non-magnetic ultrasonic motors, utilizing the expanded space of an open-bore MRI to enable use on various organs

⋆ Yu-Hsiu Lee (corresponding author) received support from the National Science and Technology Council of Taiwan under Grant NSTC 112-2628-E-002-024, NSTC 113-2628-E-002-031, as well as from the National Taiwan University Excellence Research Program, Grant 113L893901.

10.1016/j.ifacol.2025.10.194

[Chinzei et al. (2000)]. In 2007, Johns Hopkins University (JHU) in the United States developed PneuStep, a pneumatically driven harmonic gear stepper actuator, successfully implementing it in a prostate biopsy robot compatible with X-ray, CT, MRI, and ultrasound [Stoianovici et al. (2007)]. Moreover, by 2008, the German company INNOMEDIC developed the first commercially available MRI-compatible robotic system , INNOMOTION, which is driven by a pneumatic cylinder and uses optical encoders for sensing [Melzer et al. (2008)]. Similarly, the Dutch company Soteria Medical launched a needle guidance system for prostate treatment that combines pneumatic and stepper motion [Bomers et al. (2017)]. The Worcester Polytechnic Institute (WPI) in the United States developed a multi-degree-of-freedom neurosurgery robot using piezoelectric motors with customized driving electronics [Patel et al. (2020)]. Most existing studies focus on applications in the head or lower limb regions, where the closed-bore MRI system provides greater design flexibility at both ends. In contrast, fewer studies have targeted treatments in the abdomen because of the confined space (60-70 cm in diameter), as well as the respiration-induced motion of moving targets.

Passive assist devices are commonly used for instrument positioning in abdominal interventions. Devices such as SeeStar (AprioMed, Uppsala, Sweden) and Simplify (NeoRad AS, Oslo, Norway) [Kroes et al. (2013)] provide two angular degrees of freedom. However, the need for manual operation requires moving the patient in and out of the MRI multiple times for needle angle adjustments, making the procedure labor-intensive and limiting the full potential of MRI's intraoperative guidance capabilities. In [Franco et al. (2015)], a needle positioning robot with pneumatic cylinders was developed for liver ablation; however, the insertion process still requires human intervention.

This research aims to develop an MRI-guided robotic system for needle-based abdominal interventions, allowing procedures to be performed without repeatedly repositioning the patient within the MRI scanner. Figure 1 illustrates the parallelogram-based robot. The angulation module is powered by commercially available ultrasonic motors, offering a compact footprint and a high torque density [He et al. (2024)], while the needle insertion and gripping module is actuated pneumatically. Unique features of the robotic system include:

- A compact mechanism designed for decoupled attitude control, tailored to meet the workspace requirements and space constraints of abdominal interventions.
- A lightweight, pneumatically actuated needle module designed to overcome stroke length limitations through inchworm motion.

The rest of the article is organized as follows: Section II describes the robot's design and kinematics, focusing on its decoupled parallelogram-based structure and insertion module. Section III discusses the control systems for the piezoelectric and pneumatic actuators. Section IV presents preliminary results, highlighting prototyping achievements, motor control performance, and the gripping mechanism's functionality. Lastly, Section V concludes with reflections on the system's performance, key challenges, and future research directions.

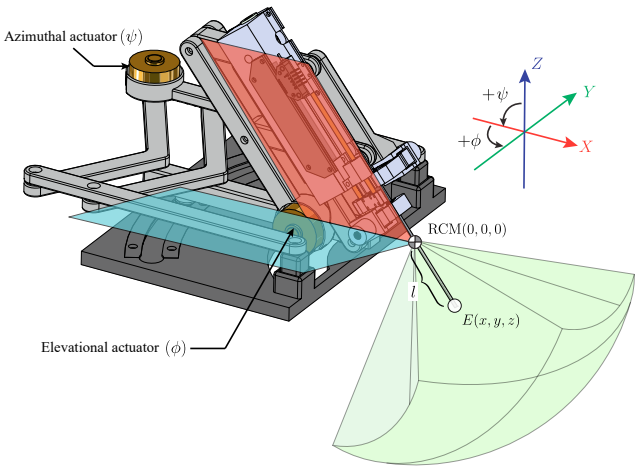

Fig. 2. The design of the robot manipulator and its RCM, which is determined by two parallelograms.

2. ROBOT DESIGN AND KINEMATICS

2.1 Decoupled Parallelogram Based Design

In robotic minimally invasive surgery, Remote Center of Motion (RCM) is a crucial and widely applied concept. It provides a fixed point in space around which the output arm can continuously rotate. By positioning the RCM at the patient's skin surface, two translational degrees of freedom are constrained, minimizing the risk of skin tearing at the entry point and enabling more stable, precise surgical movements. This setup supports faster patient recovery and reduces complications compared to traditional open surgery.

Common RCM types include isocenter, circular tracking arc, spherical linkage, and parallelogram mechanisms [Kuo et al. (2012)]. To address spatial constraints and material limitations, parallelogram-based design has been selected for the RCM mechanism. The proposed decoupled parallelogram configuration, illustrated in Figure 2, allows independent control of the elevation and azimuth angles through two separate parallelograms. This design reduces the overall footprint and simplifies control of the tool center point. Each degree of freedom is actuated by an MRI-compatible ultrasonic motor (WLG-30-R, TEKCELEO).

Figure 2 also illustrates the workspace of the robot, where the azimuth angle φ ranges from $\pm 30°$, and the elevation angle ψ ranges from $+40°$ to $-50°$. By defining the RCM as the origin of the inertial coordinate system, the inverse kinematics can be determined as follows:

$$\psi = -\cos^{-1}\left(\frac{z}{l}\right), \quad \varphi = \tan^{-1}\left(\frac{y}{x}\right) \tag{1}$$

where (x, y, z) represents the position of the end effector, and l is the insertion depth.

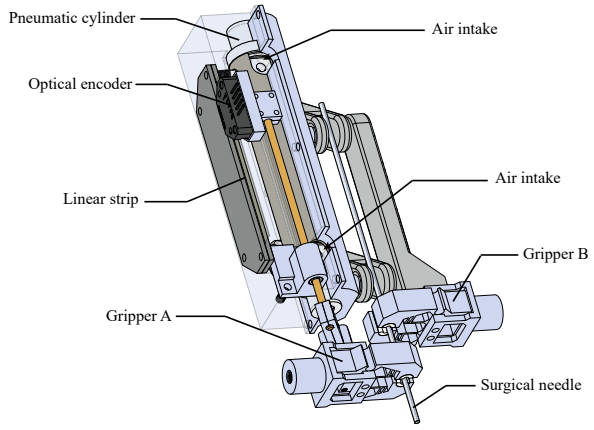

Fig. 3. The configuration of the needle insertion module components, where gripper A is actuated by the pneumatic cylinder to drive needle insertion or retraction, while gripper B is fixed in position and serves solely to hold or release the needle.

2.2 Insertion Module

The needle insertion module is shown in Figure 3. The pneumatic cylinder (Airpel E9, Airpot Co.), which features a glass cylinder bore, graphite piston, rubber seals, and a plastic housing, drives the gripper for needle insertion and retraction. It is chosen for reducing the weight of the end effector, as well as the ready availability of clean air in the equipment room of the MRI suite. The cylinder has a stroke length of 5.08 cm, which is sufficient to compensate for the typical peak-to-peak respiration-induced motion of 1.3 cm [Brandner et al. (2006)]. According to [Fischer et al. (2008)], the brass piston rod, the only metal component in this actuator, does not significantly impact MRI image quality. Additionally, a guide rod parallel to the cylinder's drive shaft is installed alongside it. A 500 lines-per-inch optical encoder (EM1, US-Digital) paired with a linear strip (LIN-500-3-0.5, US-Digital) is used for position feedback of the insertion needle.

2.3 Inchworm Motion and Gripper Design

The distance for MRI-guided liver puncture from the abdominal incision to the target tissue or lesion ranges from 28 mm to 140 mm [Hoffmann et al. (2012)]. If a pneumatic cylinder alone were used to drive needle insertion, the fully extended length of the mechanism would need to be more than twice the needle travel distance, which is undesirable given the limited design space of closed-bore MRI scanners. Building on [Pfeil et al. (2018)] and [Frishman et al. (2021)], the inchworm motion concept is introduced: intermittent reciprocating motion with shorter strokes overcomes stroke length and space constraints (Figure 4).

To provide the necessary gripping force of the inchworm motion, a pneumatically actuated gripper is designed with a compliant mechanism, which is shown in Figure 5. By applying pneumatic pressure through the inlet at the bottom, the piston shaft within the chamber, guided

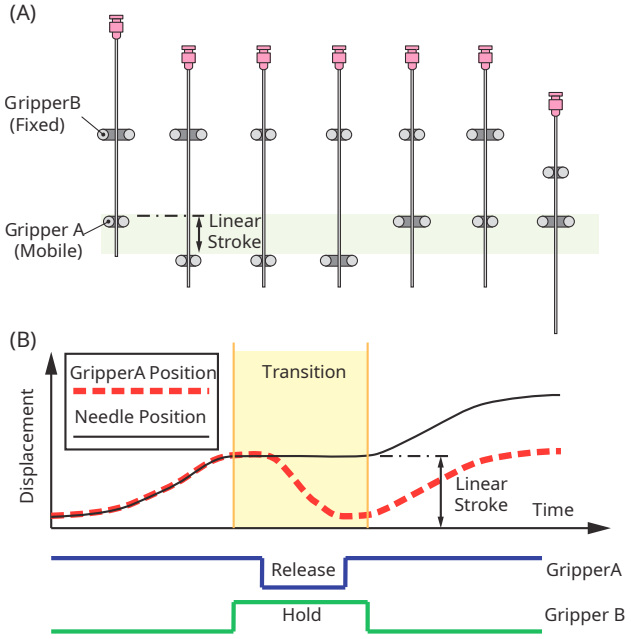

Fig. 4. Diagram of the Inchworm Motion. (a) Reciprocating needle insertion process (b) Motion relationship between gripper A and the surgical needle

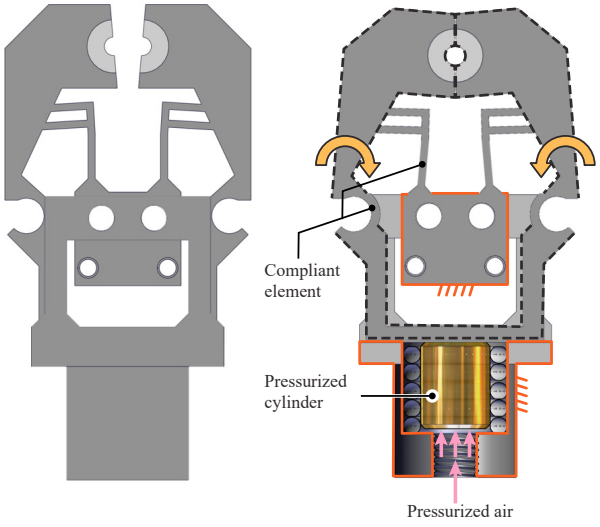

Fig. 5. Schematic of Flexible Mechanism Gripper. The red auxiliary lines highlight the part that remains stationary relative to the robot body. When the pneumatic source is activated, the brass shaft moves through the O-ring, driving the black auxiliary lines that highlight the flexible section to generate a gripping motion.

by the sealing O-ring, pushes the gripper to close and securely hold the needle at the front end. When the pneumatic pressure is released, the gripper's inherent flexibility allows it to elastically return to its original shape, thereby releasing the needle. By installing two grippers on the robot's end effector, as denoted by gripper A and gripper B in Figure 4, one can achieve the inchworm motion needed for needle insertion and retraction.

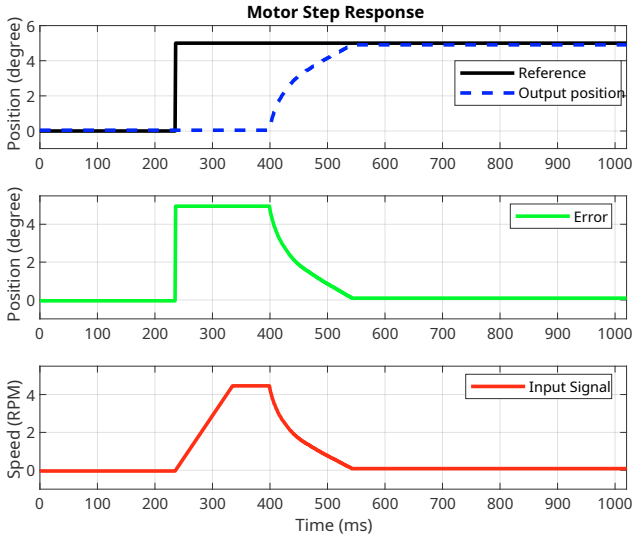

Fig. 6. Step Response of the MR-conditional ultrasonic motor.

3. ROBOT CONTROL

3.1 Ultrasonic Motor Control

Due to the presence of a strong magnetic field in the MRI environment, conventional motors that rely on electromagnetic effects are not suitable for robot actuation. In this study, ultrasonic motors (USMs) are employed due to their precision, high torque-to-size ratio, direct drive capability without the need for a high-reduction gearbox, and compatibility with the MRI environment.

The off-the-shelf USM operates in velocity mode, so a proportional controller with a gain of $K_p = 0.9$ is used for angular position control in both azimuthal and elevational actuators, despite their different characteristics, as this setting yielded satisfactory results. The step response, shown in Figure 6 with a reference angle of 5 degrees, shows a time delay of 164 ms, a rise time of 115 ms, and a steady-state error of 0.095 degrees, likely due to the dead-zone of the driving electronics or mechanical friction. The input signal, saturated at 10 rpm, is also plotted.

During surgery, the motors primarily switch between lesion locations, with the robot's posture remaining fixed during thermal ablation. Therefore, rise time and time delay have minimal impact on performance. With MRI resolutions ranging from 1 mm to 2 mm, and up to 0.5 mm for high-resolution imaging, the current steady-state error of 0.095 degrees is within acceptable limits.

3.2 Pneumatic Cylinder Control

The linear actuator of the needle insertion mechanism adopts the pneumatic cylinder mentioned in Section 2.2. A PID controller was used to achieve closed-loop control, stabilizing the system. The sampling frequency for the control system was set to 1000 Hz. The block diagram of the control system is illustrated in Figure 7

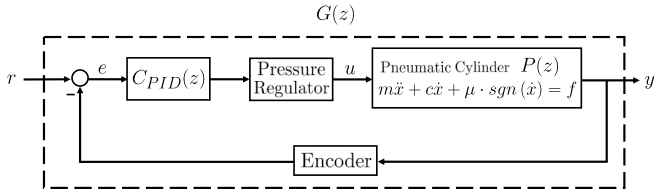

Fig. 7. Block diagram of the Insertion module.

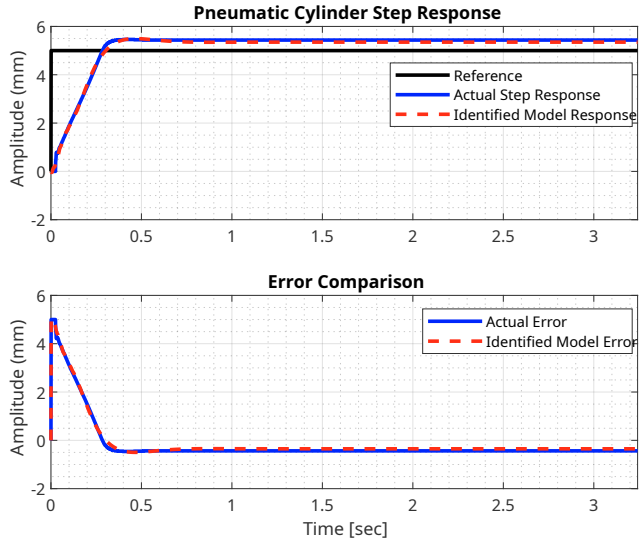

Fig. 8. Step Response of the MR-conditional pneumatic cylinder.

$$G(z) = -0.004476\frac{(z^2 - 2.0612z + 1.1506)}{(z^2 - 2.2086z + 1.4685)} \times \frac{(z^2 - 1.6208 + 0.6794)(z - 1.3897)}{(z^2 - 1.4654z + 0.6643)(z - 0.6396)(z - 1.4795)} \quad (2)$$

As shown in [Musa et al. (2021)], the pneumatic cylinder is essentially a second-order system $P(z)$. With a PID controller for feedback control, the overall system $G(z)$ becomes at least third-order. The procedure for identifying the transfer function from r to y, where r is the desired position and y is the current position of the cylinder, is outlined as follows. The system identification is performed by first obtaining the step response, which is then used to derive the Finite Impulse Response (FIR) model. Based on Ho-Kalman's algorithm [Ho and Kálmán (1966)], the first 6 dominant states from singular value analysis are preserved, rendering the transfer function model as presented in Equation 2.

As shown in Figure 8, the actual step response data and the step response of the identified system $G(z)$ are in close agreement, with a steady-state error of approximately 0.43 mm, smaller than the MRI resolution of 0.5 mm. This demonstrates the pneumatic cylinder's capability to complete the needle insertion task with the required precision.

Initially, the system exhibited significant overshoot during controller tuning. Following [Musa et al. (2021)], addi-

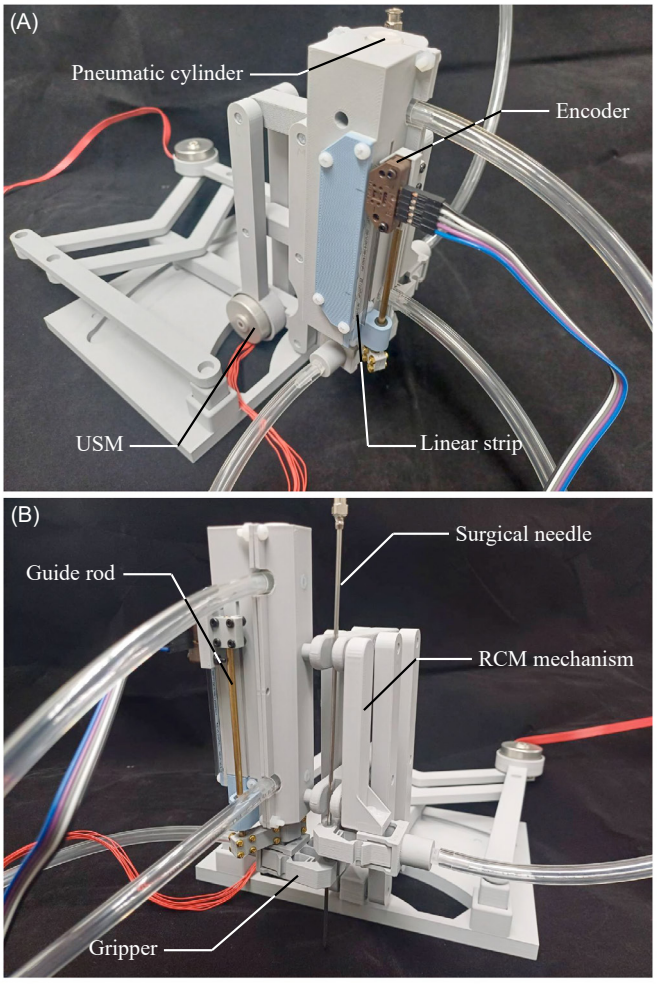

Fig. 9. The prototype of the abdominal biopsy robot. (A) Oblique overhead view (B) Oblique front view

tional friction was applied to the piston rod, effectively mitigating the overshoot and improving motion control stability for both insertion and retraction.

4. PRELIMINARY RESULTS

4.1 Prototyping

Figure 9 shows the prototype of the abdominal biopsy robot developed in this study. The main body is 3D printed, with bearings, screws, nuts, and related parts made from MRI-compatible materials like plastic or brass. Actuator cables and pneumatic tubing are extended to a safe distance to avoid interference with MRI imaging. Functional testing, including positional control and inchworm motion strategy, is currently being conducted in the laboratory.

4.2 Gripping Mechanism

According to [van Gerwen et al. (2012)], the puncture force in surgical procedures is influenced by factors like needle tip shape, diameter, insertion speed, and tissue heterogeneity, with typical forces ranging from 1 N to 10 N in porcine liver experiments.

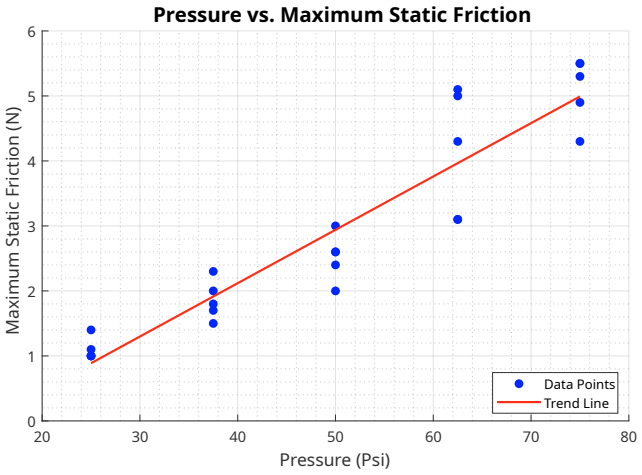

Fig. 10. Pressure vs. Maximum static Friction.

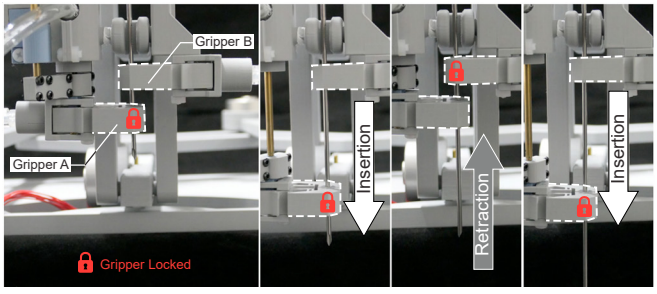

Fig. 11. The inchworm motion process.

Figure 10 shows the relationship between supply pressure and gripping force on a 14-gauge needle. Measurements indicate a positive correlation, and the prototype's gripping force meets application requirements. Ongoing research aims to further increase this force through adjustments in dimensions, materials, and surface properties.

Figure 11 illustrates the inchworm motion sequence with our needle insertion module and compliant gripper. The pneumatic cylinder controls needle insertion and retraction via an electronically controlled proportional valve, while pressure switches toggle the gripper between clamping and releasing the surgical needle.

5. CONCLUSION

This paper presents the design, implementation, and evaluation of an MRI-compatible robotic system for needle-based abdominal interventions. The system features a decoupled parallelogram-based RCM mechanism for precise needle angulation and a pneumatically actuated insertion module with a 5.08 cm stroke length, supporting inchworm motion for extended insertion range. A compliant gripper ensures secure needle manipulation, with a gripping force sufficient for puncture forces up to 5.5 N.

Preliminary results validate the feasibility of the proposed system. The prototype, fabricated using MRI-compatible materials, demonstrated stable performance under laboratory conditions. Workspace analysis revealed angulation ranges of $\pm 30^\circ$ for azimuth and $+40^\circ$ to -50° for eleva-

tion, while the insertion module accommodated respiratory motion compensation. Testing of the inchworm motion showed smooth and repeatable needle advancements, confirming the efficacy of the design.

Future efforts include characterizing positioning and dynamic tracking in clinical settings, refining control algorithms for precision, and integrating imaging feedback for real-time operation. This system addresses MRI-guided abdominal intervention challenges, enhancing safety and efficiency.

REFERENCES

Bomers, J., Yakar, D., Overduin, C., Jansen, H., van Leeuwen, P., Schouten, M., and Huisman, H. (2017). Feasibility of a 2nd generation mr-compatible manipulator for transrectal prostate biopsy guidance. *European Radiology*, 27(4), 1776–1782.

Brandner, E.D., Wu, A., Chen, Q., Heron, D.E., Huq, M.S., Yue, N., Kalnicki, S., Komanduri, K., and Burton, S. (2006). Abdominal organ motion measured using 4d ct. *International Journal of Radiation Oncology, Biology, Physics*, 65(2), 554–560. doi: 10.1016/j.ijrobp.2005.12.042.

Chinzei, K., Miller, K., Hata, N., Jolesz, F.A., and Kikinis, R. (2000). MR compatible surgical assist robot: System integration and preliminary feasibility study. In *International Conference on Medical Image Computing and Computer-Assisted Intervention*, 921–930. Springer, Berlin, Heidelberg.

Di Costanzo, G.G., Francica, G., and Pacella, C.M. (2014). Laser ablation for small hepatocellular carcinoma: state of the art and future perspectives. *World Journal of Hepatology*, 6(10), 704–715.

Dick, E.A., Taylor-Robinson, S.D., Thomas, H.C., and Hobbs, K.E.F. (2002). Ablative therapy for liver tumours. *Gut*, 50(5), 733–739.

Fischer, G.S., Iordachita, I.I., Csoma, C., Tokuda, J., DiMaio, S.P., Tempany, C.M., Hata, N., and Fichtinger, G. (2008). MRI compatibility of robot actuation techniques–a comparative study. In *Medical Image Computing and Computer-Assisted Intervention: MICCAI International Conference on Medical Image Computing and Computer-Assisted Intervention*, volume 11, Part 2, 509–517. Springer.

Franco, E., Brujic, D., Rea, M., Gedroyc, W.M., and Ristic, M. (2015). Needle-guiding robot for laser ablation of liver tumors under mri guidance. *IEEE/ASME Transactions on Mechatronics*, 21(2), 931–944.

Frishman, S., Ings, R.D., Sheth, V., Daniel, B.L., and Cutkosky, M.R. (2021). Extending reach inside the mri bore: A 7-dof, low-friction, hydrostatic teleoperator. *IEEE Transactions on Medical Robotics and Bionics*, 3(3), 701–713. doi:10.1109/TMRB.2021.3097123.

He, B., Zhao, N., Guo, D.Y., Paxson, C.H., and Fearing, R.S. (2024). Design and control of a compact series elastic actuator module for robots in mri scanners. *arXiv preprint arXiv:2406.07670*.

Ho, B. and Kálmán, R.E. (1966). Effective construction of linear state-variable models from input/output functions. *Automatisierungstechnik*, 14(1/12), 545–548.

Hoffmann, R., Thomas, C., Rempp, H., Pereira, P.L., and Clasen, S. (2012). Performing mr-guided biopsies in clinical routine: factors that influence accuracy and procedure time. *European Radiology*, 22(3), 663–671. doi:10.1007/s00330-011-2297-x.

Kim, P.N., Lee, S.I., Rhim, H., and et al. (2012). Planning ultrasound for percutaneous radiofrequency ablation to treat small (≤ 3 cm) hepatocellular carcinomas detected on computed tomography or magnetic resonance imaging: a multicenter prospective study to assess factors affecting ultrasound visibility. *Journal of Vascular and Interventional Radiology*, 23(5), 627–634.

Kroes, M.W., Busser, W.M., Hoogeveen, Y.L., and et al. (2013). Assessment of needle guidance devices for their potential to reduce fluoroscopy time and operator hand dose during c-arm cone-beam computed tomography–guided needle interventions. *Journal of Vascular and Interventional Radiology*, 24(6), 901–906.

Kuo, C.H., Dai, J.S., and Dasgupta, P. (2012). Kinematic design considerations for minimally invasive surgical robots: an overview. *International Journal of Medical Robotics and Computer Assisted Surgery*, 8(2), 127–145. doi:10.1002/rcs.453.

Melzer, A., Bock, M., Zangos, S., Remmele, T., Suess, C., Wendt, M., and Huenges, R. (2008). Innomotion for percutaneous image-guided interventions. *IEEE Engineering in Medicine and Biology Magazine*, 27(3), 66–73.

Musa, M., Sengupta, S., and Chen, Y. (2021). Design of a 6 dof parallel robot for mri-guided interventions. In *2021 International Symposium on Medical Robotics (ISMR)*, 1–7. doi:10.1109/ISMR48346.2021.9661513.

Pacella, C.M., Francica, G., and Di Costanzo, G.G. (2011). Laser ablation for small hepatocellular carcinoma. *Radiology Research and Practice*, 2011.

Patel, N.A., Rac, M., Uneri, A., Menard, C., Lo, S., Pezeshkian, P., Hashizume, R., Arif, O., Mahesh, M., Wolinsky, J.P., et al. (2020). An integrated robotic system for mri-guided neuroablation: Preclinical evaluation. *IEEE Transactions on Biomedical Engineering*, 67(10), 2990–2999.

Pfeil, A., Andrikopoulos, G., Nikou, A., Stilli, A., De Momi, E., Faragasso, A., Loizou, P., and Georgilas, I.M. (2018). A 3d-printed needle driver based on auxetic structure and inchworm kinematics. In *International Design Engineering Technical Conferences and Computers and Information in Engineering Conference*, volume 51807. American Society of Mechanical Engineers.

Stoianovici, D., Patriciu, A., Mazilu, D., Petrisor, D., and Kavoussi, L.R. (2007). "mri stealth" robot for prostate interventions. *Minimally Invasive Therapy & Allied Technologies*, 16(4), 241–248.

van Gerwen, D.J., Dankelman, J., and van den Dobbelsteen, J.J. (2012). Needle–tissue interaction forces – a survey of experimental data. *Medical Engineering & Physics*, 34(6), 665–680. doi: 10.1016/j.medengphy.2012.04.007.